Ultrasound triggered microbubble destruction for targeted delivery of miRNA-therapeutics

Kwekkeboom, R.F.J.

2017

document version
Publisher's PDF, also known as Version of record

Increased local delivery of antagomir therapeutics to the rodent myocardium using ultrasound and microbubbles

Published in Journal of Controlled Release Vol. 222, pp. 18-31, 2016

Rick F.J. Kwekkeboom [1,4],
Joost P.G. Sluijter [2],
Ben J. van Middelaar [2],
Corina H. Metz [2],
Maike A. Brans [2],
Otto Kamp [3,4],
Walter J. Paulus [1,4],
René J.P.Musters [1,4]

[1] *Department of Physiology, VU University Medical Center, Van der Boechorststraat 7, 1081 BT Amsterdam, The Netherlands*
[2] *Department of Experimental Cardiology, University Medical Center Utrecht, P.O. Box 85500, 3508 GA, Utrecht, The Netherlands*
[3] *Department of Cardiology, VU University Medical Center, De Boelelaan 1117, 1081 HV Amsterdam, The Netherlands*
[4] *Institute for Cardiovascular Research-VU (ICaR-VU), VU University Medical Center, Van der Boechorststraat 7, 1081 BT Amsterdam, The Netherlands*

4

Abstract

Recent developments in microRNA (miRNA) research have identified these as important mediators in the pathophysiological response upon myocardial infarction (MI). Specific miRNAs can inhibit the translation of entire groups of mRNAs, which are involved in specific processes in the pathophysiology after MI, e.g. the fibrotic, apoptotic or angiogenic response. By modulating miRNAs in the heart, these processes can be tuned to improve cardiac function. Antagomirs are effective miRNA-inhibitors, but have a low myocardial specificity and cardiac antagomir treatment therefore requires high doses, which causes side effects. In the present study, ultrasoundtriggered microbubble destruction (UTMD)was studied to increase specific delivery of antagomir to the myocardium. Healthy control mice were treated with UTMD and sacrificed at 30 min, 24 h and 48 h, after which antagomir delivery in the heart was analyzed, both qualitatively and quantitatively. Additionally, potential harmful effects of treatment were analyzed by monitoring ECG, analyzing neutrophil invasion and cell death in the heart, and measuring troponin I after treatment. Finally, UTMD was tested for delivery of antagomir in a model of ischemia–reperfusion (I/R) injury. We found that UTMD can significantly increase local antagomir delivery to the non-ischemic heartwith modest side-effects like neutrophil invasion without causing apoptosis. Delivered antagomirs enter cardiomyocyteswithin 30 min after treatment and remains there for at least 48 h. Interestingly, after I/R injury antagomir already readily enters the infarcted zone and we observed no additional benefit of UTMD for antagomir delivery. This study is the first to explore cardiac antagomir delivery using UTMD. In addition, it is the first to study tissue distribution of short RNA based therapeutics (~22 base pairs) at both the cellular and organ levels after UTMD to the heart in general. In summary, UTMD provides a myocardial delivery strategy for non-vascular permeable cardiac conditions later in the I/R response or chronic conditions like cardiac hypertrophy.

Key words: Ultrasound, Microbubbles, MicroRNA, Antagomir, Drug delivery, Ischemia reperfusion, Cardiovascular.

Introduction

Since the discovery of microRNAs (miRNAs) in humans [1], many of these small non-coding RNA molecules have been found to be involved in progressive pathological conditions, including several cardiac diseases [2]. miRNAs are small RNA molecules that bind to the 3' untranslated region of mRNA molecules and thereby block their translation. One miRNA can potentially bind to whole groups of mRNA targets that are directly involved in specific processes like apoptosis, angiogenesis or fibrosis formation [3]. Blocking the functionality of specific miRNAs has been feasible for several years [4] and by this approach cardiac function was improved in several models of disease [5,6]. However, current approaches that use miRNA inhibitors have low organ specificity [7] and therefore employ high doses, making side effects and cost an issue and creating the need for better delivery strategies. One such delivery strategy is the use of gas-filled microbubbles (MB) in combination with ultrasound (US) [8]. Intravascular MB can, upon destruction by US Triggered MB Destruction (UTMD), locally increase vascular permeability and cellular membrane permeability [9,10]. Several studies have successfully delivered plasmid DNA specifically to the heart to improve cardiac function [11–13]. As this strategy has also been used to locally deliver siRNA as a proof of concept [14], UTMD is an interesting option to increase cardiac local delivery of miRNA inhibitors due to similarities in chemical structure with siRNAs. In this study, we hypothesized that UTMD can be used to increase antagomir inhibitor delivery to the healthy and diseased hearts. Antagomirs are single stranded, 2'-O-methyl and phosphorothioate linked oligoribonucleotides with a sequence that is exactly complementary to its miRNA-target and a cholesterol attached to the 3' end. As a highly relevant cardiac disease we choose a model of ischemia–reperfusion (I/R) to test UTMD effectivity. We investigated the localization of these delivered antagomirs at both the whole organ as well as at the cellular level to determine feasible cellular targets for miRNA modulation, specific for UTMD. In addition, we determined the localization of delivered antagomir over time (up to 48 h) and investigated the acute functional response of the heart to UTMD and the later (patho) physiological response of the heart to UTMD at a cellular level.

Materials and methods

Antagomir–microbubble preparation

Cationic microbubbles (cMB) were produced as described previously [15]. Briefly, a combination of 1,2-distearoyl-sn-glycero-3- phosphocholine (Avanti Polar Lipids, Alabaster, LA, USA), 1,2-stearoyl-3-trimethylammonnium-propane (Avanti Polar Lipids) and polyoxyethylene-40-stearate (Life Technologies, Bleiswijk, TheNetherlands), in a molecular ratio of 2:1:0.6, was solved in a H2O(l), glycerol (Life technologies), propylene glycol (Sigma-Aldrich, Zwijndrecht, The Netherlands) mixture (volume 24:13:3) in a 2 ml tube with perfluorobutane gas

(C4F10(g)¸ F2 Chemicals, Lancashire, UK) in the capspace. cMB were produced by means of mechanical agitation using a Vialmix™(Lantheus Medical Imaging, North Billerica, MA, USA) high-speed shaker. Subsequently, cMB were washed 3 times using centrifugal flotation. Size distribution and amount of washed cMB were determined using a Multisizer 3' (Beckman Coulter Nederland, Woerden, Netherlands) and concentrated to 2 * 10_9 cMB/ml in H_2O for in vivo experiments. Antagomir formulation for analysis time points 30 min and 24 h was Cy3-5'-a*c*ucccugccuuucccuua*u*g*u*-3'-cholesterol. For the 48 h timepoint it was Cy3-5'-a*c*ugccugucugugccugc*u*g*u*-3'-cholesterol. Antagomirs are 3' cholesterol modificated, 2'-O-methylated, and contain PTO-linkages (*) at the first two and last four nucleotides. Antagomirs were custom-ordered from VBC-Biotech, Vienna, Austria as reported before [16]. Prior to UTMD treatment, 2 nmol of antagomir was added to 200 * 10_6 cMB in 100 µl H_2O at room temperature and incubated for 5 min to bind the negatively charged antagomir to the cationic MB through electrostatic interactions prior to i.v. tail vein injection.

Animal experiments

All animal experiments were approved by the institutional Animal Experimentation Committee of Utrecht University.

AntagomiR delivery to the healthy myocardium

Male C57BL/6 mice (n = 50, 20–24 g; Harlan, Horst, Netherlands) were anesthetized with aerosol anesthetic isoflurane. Subsequently, mice were placed on a heating pad while their temperature was being monitored and maintained at 37 °C. Mice received a bolus i.v. injection of 0.75 mg/kg bodyweight of antagomir either combined with 200 * 10^6 cMB in 100 µl H2Oorwith100 µl H2O alone for control animals. After i.v. injection, mice hearts were treated locally with high intensity US using a Philips Sonos 5500 with either an S12 or S3 transducer in short axis view (Fig. 1) with different treatment protocols (Table 1). Both the S12 and S3 transducer were coupled to the mouse skin by US transmission gel (Aquasonic 100, Parker Labs, NJ, USA). For the S3 transducer (1.5 MHz), the distance between the transducer and murine heart was 4 cm and machine settings for focus and depth were set to 4 cm and 9 cm respectively. Focus is the distance from the surface of the transducer at which the US picture is clearest and depth is the maximum distance that is visualized on the US machine. For the S12 transducer (7 MHz) the distance between US-transducer and murine heart was 1.5 cm, regardless of the focus settings on the US machine. For the S12 B-mode treatment protocol, two imaging settings of the Sonos 5500 were used. For the S12 B-mode 1 protocol, the machine was set to the Fusion 1 setting, and for the S12 B-mode 2 protocol, the machine was set to the Fusion 5 setting. Fusion 1 and Fusion 5 are Philips Sonos specific settings that determine the frequency that is received by the US transducer for image processing. The Fusion 1 settings receive and process frequencies closer to 6 MHz while the Fusion 5 settings receive and process frequencies closer to the 8MHz. In addition to S12 B-mode protocols, mice were also treated with S12

Power Doppler protocols as Power Doppler employs longer US pulses (B-mode delivers two waves per pulse versus Power Doppler that deliver 6–8 waves per pulse), which is expected to result in more robust local delivery. Two different S12 Power Doppler treatment protocols were used. The S12 Power Doppler 1 protocol employed an MI of 1.5 and a focus and depth at 1.5 cm and 9 cm respectively. The S12 Power Doppler 2 protocol used identical settings with the except the settings for focus and depth, these were 3 cm and 16 cm. As this focus and depth are higher, the Sonos machine automatically increases the amount of US pulses that the transducer transmits and decreases the US-frequency to 6 MHz. The S12 Power Doppler 2 protocol thus employs the same MI and frequency, but a higher amount of US-pulses per second. Murine hearts were treated with US for 1 s every 10 s for 15 min. Treated mice were sacrificed 30 min, 24 h or 48 h after treatment after which the hearts were embedded in Tissue Tek O.C.T. Compound (VWR International B.V., Amsterdam, The Netherlands), frozen in liquid nitrogen and whole blood was taken for further analysis. Prior to, directly after treatment, and at the moment of sacrifice, cardiac function was measured in M-mode by means of echocardiography (Vevo 2100, Visualsonics, Amsterdam, The Netherlands). To determine the direct effect of treatment on cardiac function, the difference between before and after treatment was calculated for measured left ventricular diameter, heart rate, fractional shortening, and ventricular wall thickness and for calculated left ventricular volumes, ejection fraction, and cardiac output. Additionally, the ECG was recorded before, during and directly after treatment.

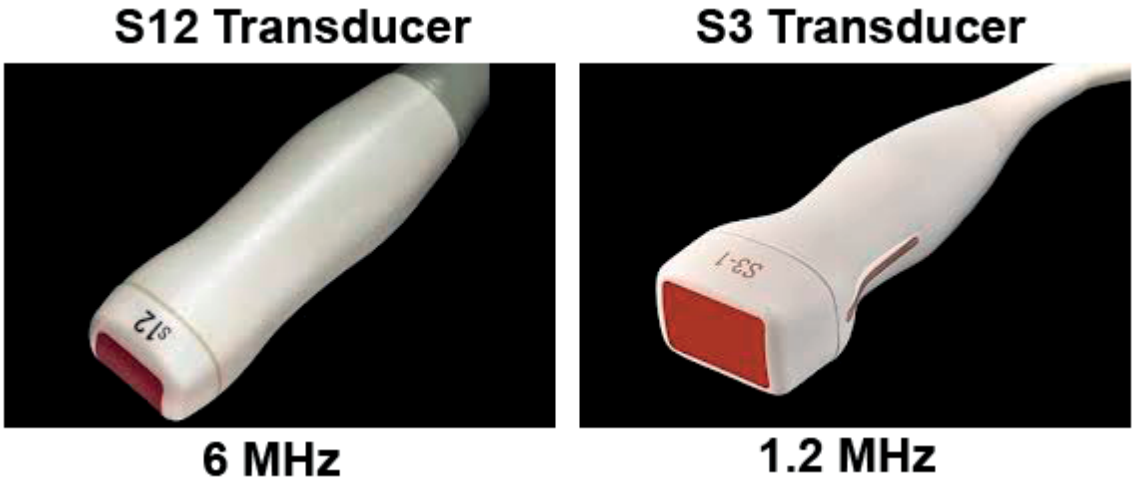

Figure 1 Used US-transducers for UTMD. *A) Transducers operate at different frequencies as displayed below the images. The S3 transducer has an imaging surface which is 4× as large as the S12 transducer, making it more difficult to precisely place the transducer over a mouse heart. B) The dotted red line represents the imaging/treatment plane that was used for UTMD.*

AntagomiR delivery to ischemia-reperfusion myocardium

For delivery experiments on the ischemia–reperfusion (I/R) hearts, mice were anesthetized with an intraperitoneal injection of a mixture of Fentanyl (0.05 mg/kg), Dormicum (5 mg/

kg) and Domitor (0.5 mg/kg). Mice were intubated and ventilated with a gas mixture of 96% oxygen and 4% nitrogen. The left coronary artery (LCA) was ligated with an 8-0 vicryl suture with a section of polyethylene-10 tubing placed over the LCA. After 30 min, reperfusion was initiated by releasing the ligature and tubing as described before [17].Within 5 min of the initiation of reperfusion, mice received an i.v. injection of 0.75 mg/kg body weight antagomir in 100 µl H2O either with cMB (2 * 10_8 in total) or without cMB for control animals. Subsequently, the S12 transducer was placed on the heart and mice were treated with the S12 Doppler protocol B as described in Table 1. Mice were sacrificed either 30 min or 24 h after treatment at which point the heart was collected for further analysis.

Qualitative immunofluorescence microscopy

Wheat germ agglutinin-staining and montage-imaging

Myocardial cryosections, 10 µm thick, were fixed in 4% paraformaldehyde in PBS for 5 min. Subsequently, sections were permeabilized using 0.01% vol. triton x-100 (Sigma-Aldrich) in PBS and stained with 50 µl wheat germ agglutinin (WGA) Alexa Fluor 488 Conjugate solution (1 µg/ml, Life technologies) and enclosed with mounting medium containing DAPI (Vector Labs, Peterborough, UK) for nuclear staining. Next, sections were visualized on a ZEISS Axiovert Marianas 200 M inverted fluorescence microscope (Intelligent Imaging Innovations, Denver, CO, USA) with DAPI, FITC and cy3 filter sets. Of these sections, montage images of the whole heart were made by stitching separate images taken at 200× magnification to determine localization at the organ level. For localization at the cellular level, 400× high-magnification images were taken.

CD31-staining

For the 30 minute time point, cryosections were stained for CD31 using immunofluorescence. Sections were fixed in 4% paraformaldehyde in phosphate buffered saline (PBS) for 5 min. Subsequently, sections were permeabilized using 0.01% vol. triton x-100 and incubated with 100 µl of polyclonal primary antibody against CD31 (2 µg/ml, sc-1506, PECAM-1 (M-20), Santa Cruz, Dallas, TX, USA) over night at 4 °C in PBS with 1% bovine serum albumin (BSA). Subsequently, 100 µl of secondary antibody with conjugated Alexa Fluor 488 dye was added (Life Technologies) for 30 min at room temperature (RT) in PBS with 1% BSA, sections were enclosed with mounting medium containing DAPI for nuclear staining (Vector Labs). Subsequently, sections were visualized at 400×magnificationwith DAPI, FITC and cy3 filters. Negative controls for the staining, using only the secondary antibody, were performed to correct for nonspecific binding .

TUNEL-staining

To detect cell death at 24 h and 48 h, cryosections were stained with a fluorescein in situ cell death detection kit TUNEL assay according to manufacturer's instructions (Roche, Cat no.:

11 684 795 910, Woerden, The Netherlands) and Hoechst counter stain for nuclei. Sections were analyzed with a ZEISS Axiovert Marianas 200 M inverted fluorescence microscope at 200× magnification.

Neutrophil-staining

To study neutrophil infiltration, cryosections were fixed in acetone, incubated with Avidin (Biotin Blocking system, Dako, Heverlee, Belgium) for 15 min, washed with PBS 3 times, subsequently incubated with biotin (Biotin Blocking system) and washed with PBS 3 times. Next, sections were washed with PBS containing 0.05% vol. TWEEN and incubated in normal goat serum for 30min. Then, sections were incubated with 100 µl of primary antibody against Ly-6G ((1.25 µg/ml) Biolegend, Fell, Germany) in PBS containing 0.1% bovine serum albumin (BSA) for 60 min. at RT, washed 3 times with PBS and, subsequently, incubated with a biotinylated secondary goat-anti-rat antibody (Southern biotech, Birmingham, AL, USA) in PBS with 1% BSA for 30 min. at RT.

Sections were then washed 3 times with PBS and incubated with streptavidin-FITC (Biolegend) in PBS for 60 min. at room temperature. Finally, sections were washed 3 times, counterstained with Hoechst nuclear staining and enclosed in mounting medium. Negative controls for the staining, using only the secondary antibody, were performed to correct for non-specific binding .

Quantitative fluorescence microscopy

Frozen hearts were sectioned in slices of 10 µm from apex to base in the transversal plane. Immediately after sectioning, pictures of 10 slices per mouse were taken at 100× magnification on the ZEISS Axiovert Marianas 200 M. Pictures were taken with a 10× air objective, constant illumination time of 1000 ms, constant settings on the CCD-detector, and constant pixel size. Pictures were subsequently analyzed using Slidebook 5.5 Software (Intelligent Imaging Innovations). A digital overlay mask of the cy3-channel (antagomir signal) was created with a lower cut-off (threshold) value set at 100 a.u. intensity and a maximum cut-off value set at 4095 a.u. (which was the sensitivity limit of the camera). The auto-fluorescence of murine hearts was determined by imaging sections of 4 untreated murine hearts and defined the average cy3-channel intensity as the lower cut-off (threshold). Of this mask the Mean intensity, Median intensity, Maximal intensity, Sum intensity and Surface area above threshold of the mask were calculated as read-out parameters for the effect of US and cMB treatment on antagomir delivery to the heart (for an in detail description of these parameters we refer to the supplementary data). It is important to note that only the readout parameters Sum intensity and Surface area above threshold directly represent increased tissue delivery of antagomir. The other read-out parameters Mean intensity, Median intensity and Max intensity give information about distribution of antagomir through the section. To

compare groups, sections 2400–3100 µm away from the apex were used since that part of the heart was in the US-beam during treatment.

Troponin I ELISA

Troponin I levels were determined in whole blood taken from mice with a high sensitivity ELISA kit following the manufacturer's instructions (Life Diagnostics, Cat. No: CTNI-1-HS, West Chester, PA, USA). For the blood collected 30 min after treatment, Troponin I levels were correlated to the quantification of antagomir delivery to the heart using the Pearson correlation test.

Statistical analysis

Statistical analysis was performed with Prism5 (Graphpad Software, La Jolla, CA, USA). Means of different treatment groups were tested for statistical difference compared to the untreated control group with a student's t-test and considered significantly different at $p < 0.05$.

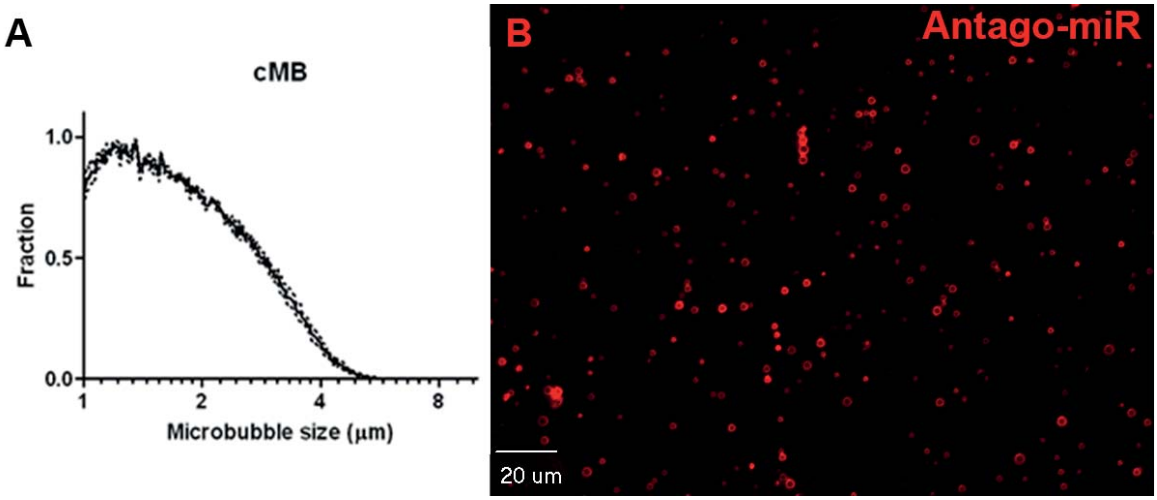

Figure 2 Cationic microbubble size distribution and antagomir attachment. *A) Graph ofmicrobubble size distribution. On the x-axis the microbubble diameter is depicted. On the y-axis, the amount of microbubbles of a particular size is displayed as a fraction of the most-abundant size. B) Fluorescence microscope image of antagomir bound to cationic microbubbles.*

Results

Microbubble preparation and antagomir binding

As we described before, prepared cMB had a mean diameter of 1.77 µm (Fig 2A) and antagomir was successfully attached to the MB shell through electrostatic interactions during a 5 minute incubation time (Fig 2B).

Delivery of antagomiR to the healthy myocardium

Localization of antagomiR (30 min)

Upon a single i.v. injection of 0.75 mg/kg antagomir, no fluorescent antagomir signal could be observed in the hearts of the control group (Fig. 3A+F) 30 min after treatment. After injection of cMB with antagomir, US treatment increased delivery of antagomir to the myocardium (Fig. 3B–E+G–I) across all treatment groups. For the S12 B-mode 1 protocol, however, this effect was mild (Fig 3B). The results with the S12 B-mode 2 protocol were heterogeneous; in 2 out of 6 mice delivery was profound (Fig. 3C),while in the remaining mice antagomir delivery was mild (Fig. 3D). The qualitative results of the S3 Power Doppler protocol were more reproducible, leading to increased delivery to cardiomyocytes in all mice (Fig. 3E). Additionally, with the S12 Bmode protocols, delivery was restricted to the anterior wall of the heart (Fig. 3C+D). Interestingly, antagomir delivery was not restricted to the anterior wall of the heart when the S3 Power Doppler protocol was used. However, in the S3 Power Doppler group, localization of antagomir delivery was not uniforma nd the extent of delivery was heterogeneous as well. High-magnification images revealed that all delivered antagomir in the S12 B-mode 1 group was localized directly around the capillaries (Fig. 3G). The cellular delivery pattern of S12 B-mode 2 and S3 Power Doppler were comparable and antagomir could be found inside cardiomyocytes (Fig. 3H+I). Strikingly, cardiomyocytes either turned entirely red or did not show any intracellular antagomir signal at all, indicating an on-or-off reaction of cardiomyocytes to the treatment.

Quantification of local delivery (30 min)

Quantification of increased delivery revealed that UTMD treatment influenced antagomir delivery to the heart in several quantitative parameters (Fig. 3J–N). UTMD with S12 B-mode 2 and S3 Power Doppler significantly increased the Mean intensity (Fig. 3J) and Max intensity (Fig. 3L) compared to control animals ($p < 0.05$), indicating an effect on distribution pattern of delivered antagomir as a result of UTMD. Additionally, UTMD with S12 B-mode 2 and S3 Power Doppler significantly increased Sum intensity (Fig. 3M) and Surface area above threshold (Fig. 3N) ($p < 0.05$), which indicates an absolute increase in antagomir delivery to the myocardium.

Localization of antagomiR (24 h)

After 24 h, antagomir fluorescent signal could still be observed in the hearts of US and cMB treated mice (Fig 4B+C) but not in control animals (Fig. 4A). Treatment with the S3 Power Doppler protocol led to antagomir delivery to the anterior left ventricular wall, the septum and the posterior wall (Fig 4B). As S3 Power Doppler treatment was most successful at 30 min we added a treatment protocol with S12 Power Doppler for analysis at 24 h. The S12 Power Doppler transducer is smaller compared to the S3 transducer, which allows for more precise

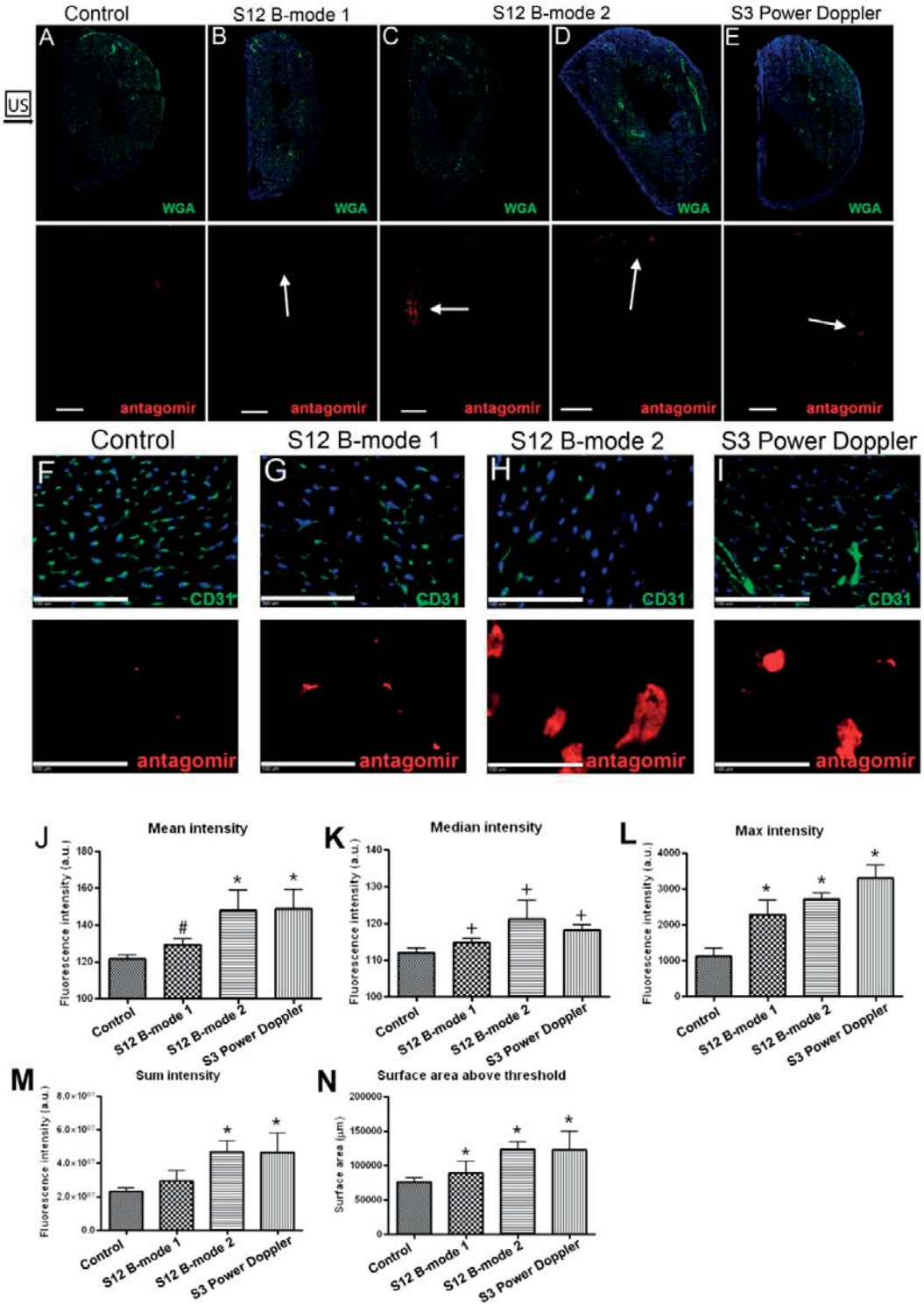

Figure 3 UTMD-triggered antagomir delivery to the healthy myocardium after 30 min. *A–E) Montage images of hearts extracted 30 min after UTMD, stained with wheat germ agglutinin (green) and DAPI (blue). The antagomir is visualized in red. Arrows point toward the part of the heart where the UTMD effect was observed. Size bar=1mm. F–I) Higher magnification images with CD31 staining (green) and DAPI staining (blue). Antagomir is visualized in red. Size bar= 100 µm. J–N) Quantification of fluorescence images. *p < 0.05, +p < 0.01, #p =0.06 compared to control values. Amount of animals per group: control=6, S12 B-mode 1=5, S12 B-mode 2=6, S3 Power Doppler=3. Control animals received an i.v. injection of antagomir only and were treated with the S3 Power Doppler protocol.*

placement on the heart. 24 h after As with S3 Power Doppler treatment, S12 Power Doppler 1 treatment increased delivery of antagomir to the heart (Fig. 4C). High-magnification images revealed that for both treatment protocols, at a cellular level, antagomir delivery was similar (Fig. 4D–G). The same on-or-off uptake response in cardiomyocytes of antagomir was observed at 24 h. No difference in cellular localization was observed between the S3 Power Doppler (Fig. 4D+E) and S12 Power Doppler protocols (Fig. 4F+G). Two distinct morphological patterns of cellular antagomir delivery were observed. First, antagomir delivery was observed in areas with a high density of cells, indicating intracellular and extracellular antagomir delivery (Fig. 4H+I, arrow-heads). Second, antagomir delivery was observed into cardiomyocytes displaying a normal morphology and no influx of cells (Fig. 4J+K, arrows). A part of the influx of cells was identified as neutrophils (Fig. 4M+O). However, not all invading cells could be identified; possible other candidates are monocytes and lymphocytes. Additionally, only in some areas antagomir delivery was found in combination with an influx of neutrophils (Fig 4M+O), in some other areas no neutrophils could be found around spots of antagomir delivery (Fig 4L+N). Finally, independent of delivery pattern, no apoptosis was observed in all animal groups (Fig. 4P–S). As positive control, I/R mouse hearts were stained with the same TUNEL procedure. Apoptosis was clearly visible in those hearts as can be seen in Fig. 8.

Quantification of local delivery

Quantification of microscopy images at 24 h revealed that UTMD treatment of micewith S3 or S12 Power Doppler 1 protocols significantly increased Mean intensity (Fig. 4T), Median intensity (Fig. 4U), Max intensity (Fig. 4V), Sum intensity (Fig. 4W) and Surface area above threshold (Fig. 4X) compared to control animals ($p < 0.05$), meaning that UTMD both had an effect on antagomir delivery pattern (indicated by parameters Mean intensity, Median intensity, and Max intensity) and caused an absolute increase of antagomir delivery to the myocardium (indicated by parameters Sum intensity and Surface area above threshold). Treatment with S12 Power Doppler showed the most homogeneous delivery results.

Localization of antagomiR (48 h)

48 h after treatment, no antagomir could be seen in the myocardium in control animals (Fig. 5A). As the S12 Power Doppler 1 treatment gave the most reproducible results at 24 h, we used this protocol for delivery at 48 h. At 48 h, antagomir delivery to the anterior wall of the left ventricle was increased with S12 Power Doppler 1 treatment; however, the increase was modest (Fig. 5B). In an effort to further increase delivery, the US-intensity was increased, the resulting US-protocol Power Doppler 2 increased the area of the heart in which the US and cMB effect could be observed (Fig. 4C). S12 Power Doppler 2 had a higher setting for depth and focus compared to S12 Power Doppler 1, resulting in a larger pulse length of emitted US, a slightly lower frequency (6 MHz for S12 Power Doppler 2 compared to 7 MHz for Power

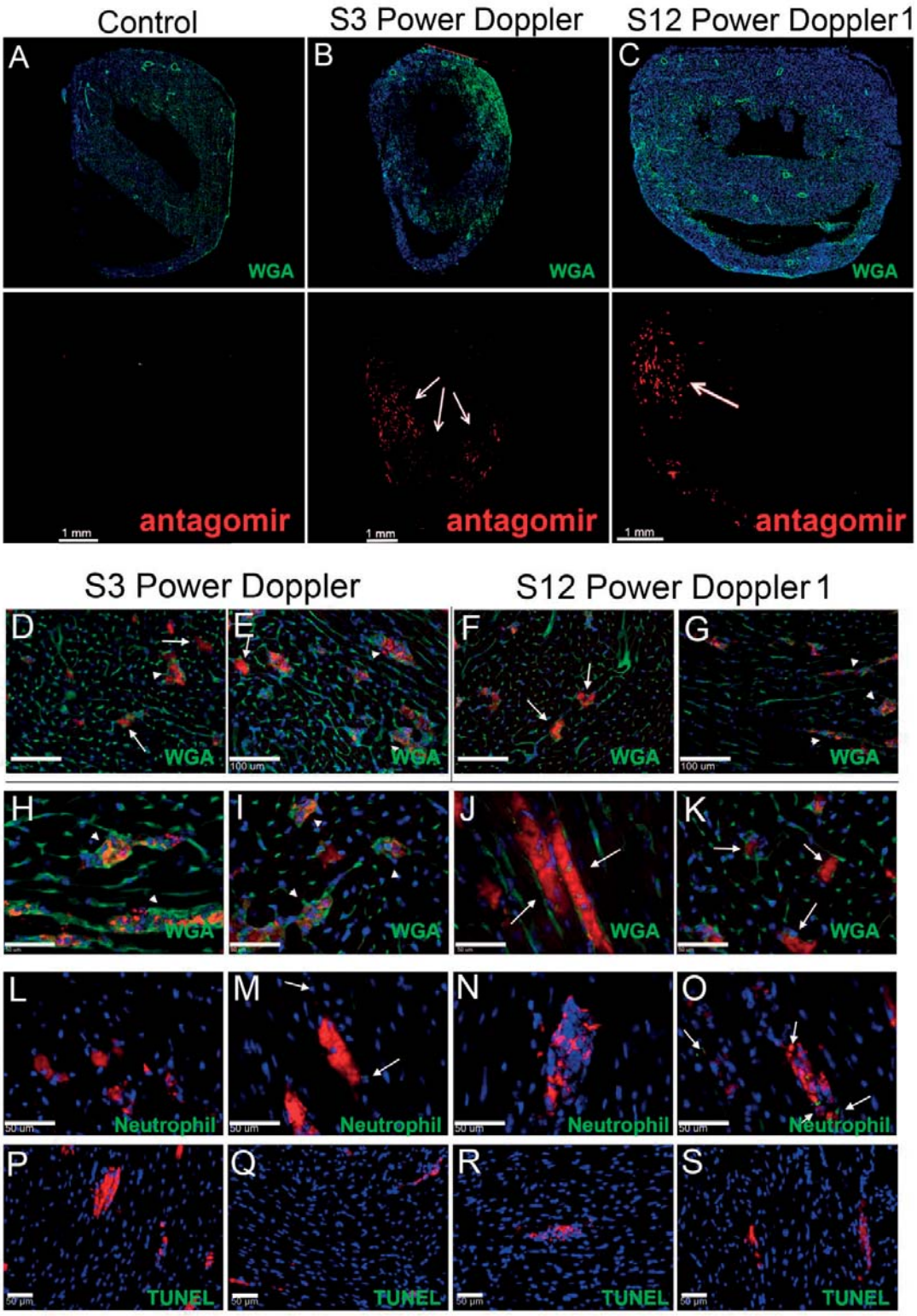

Figure 4 UTMD-triggered antagomir delivery to the healthy heart after 24 h.

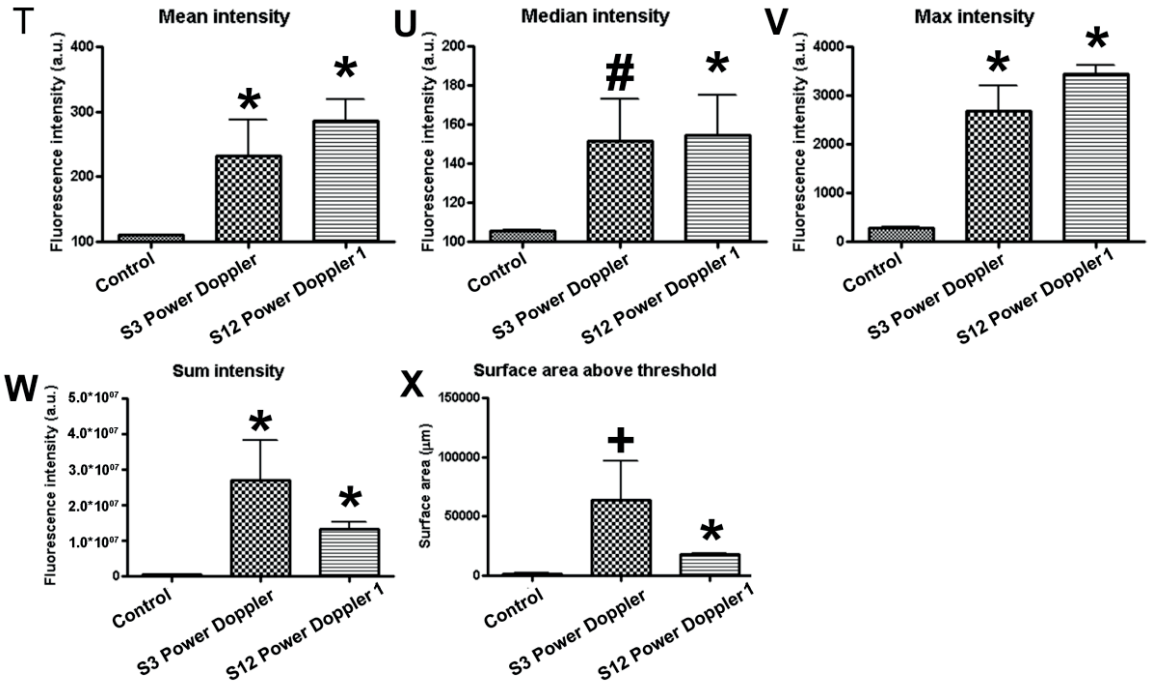

Figure 4 UTMD-triggered antagomir delivery to the healthy heart after 24 h. (continued)
*A–C) Montage images of hearts extracted 24 h after treatment, stained with wheat germ agglutinin (green) and DAPI (blue), antagomir is visualized in red. Arrows point toward the part of the heart where the UTMD effect was observed. Size bar= 1 mm. D–G) Fluorescence microscopy images of cryosections of hearts treated with either S3 Power Doppler UTMD or S12 Power Doppler UTMD, stained with wheat germ agglutinin (green) and DAPI (blue), antagomir is visualized in red. Solid line arrows point toward intracellular delivery of antagomir-with undisturbed cardiomyocytemorphology. Arrowheads point toward intracellular delivery of antagomir accompanied by an increased density of nuclei. Size bar=100 µm.H–K) Images of hearts treated with S12 Power Doppler protocol, stainedwithwheat germ agglutinin (green) and DAPI (blue), antagomir is visualized in red. Arrowheads point toward intracellular delivery of antagomir accompanied by an increased density of nuclei (H+I). Solid line arrows point toward intracellular delivery of antagomirwith undisturbed cardiomyocyte morphology (J+K). Size bar=50 µm. L–O). Neutrophil staining (green) of S12 Power Doppler treatedmice with nuclei in blue and antagomir in red. Arrows point toward neutrophils. Size bar=50 µm. P–S) TUNEL-staining (green) of S12 Power Doppler 1 treatedmice with nuclei in blue and antagomir in red. Size bar=50 µm. T–X)Quantification of fluorescence images. *p < 0.05,+p < 0.01, #p=0.06 compared to control values.Amount of animals per group: control=5, S3 Power Doppler=5, S12 Power Doppler 1 = 3. Control animals received an i.v. injection of antagomir only and were treated with the S3 Power Doppler protocol.*

Doppler 1), and thus a higher US intensity. Importantly, at 48 h, the two distinct patterns of antagomir delivery could still be observed (Fig. 5D–G, arrowhead for pixilated pattern, arrows for normal morphology). As after 24 h, antagomir delivery at 48 h was sometimes accompanied by a modest influx of neutrophils (Fig. 5L–O). Furthermore, since this influx of neutrophils might suggest that apoptosis was induced in cardiomyocytes upon the treatment we tested this by TUNEL staining. Apoptosis was mostly not detected, only in few mice very low numbers of apoptotic cells (2/3 per imaging field) could be observed (Fig. 5P–S).

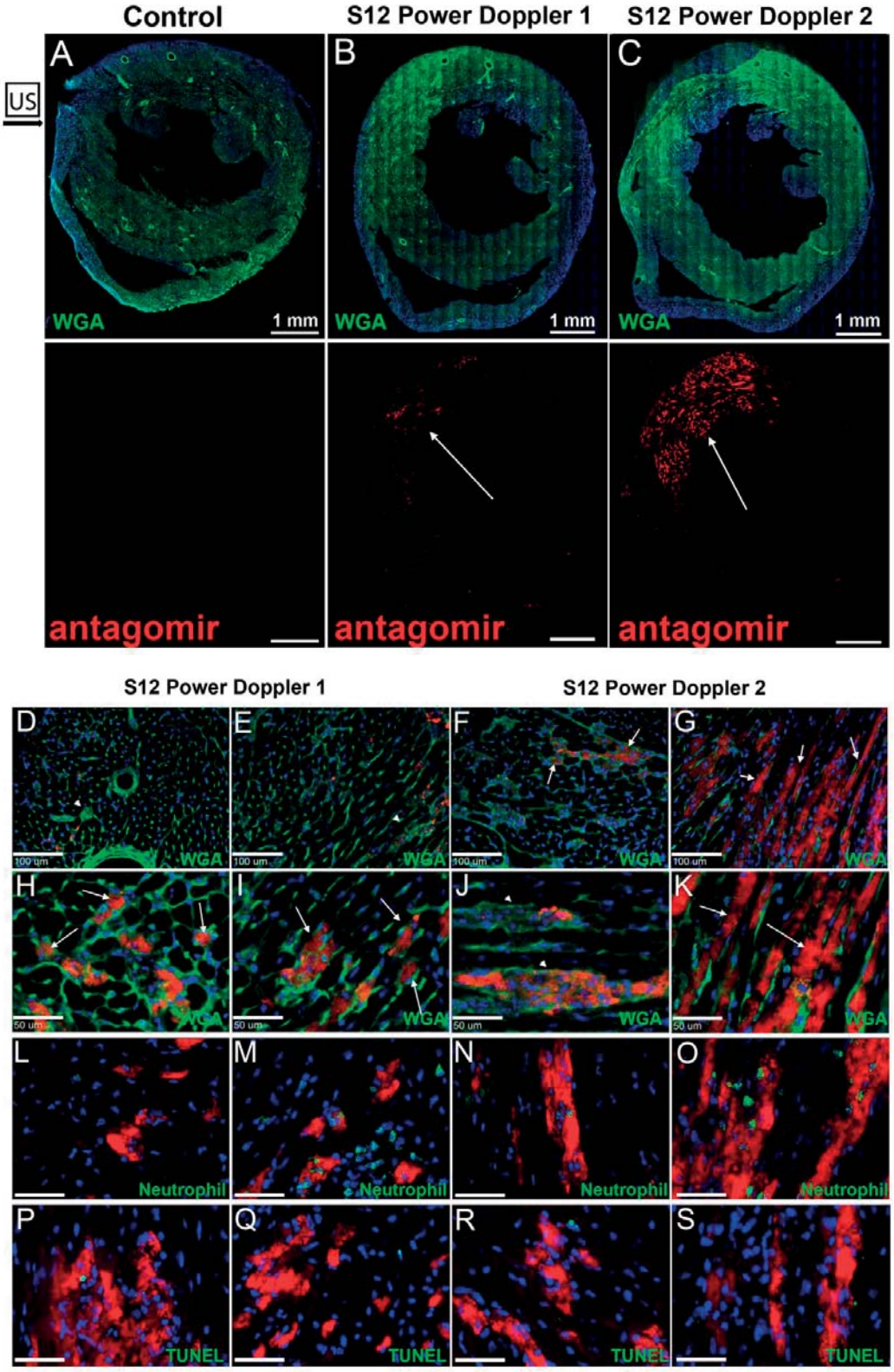

Figure 5 UTMD-triggered antagomir delivery to the healthy heart after 48 h.

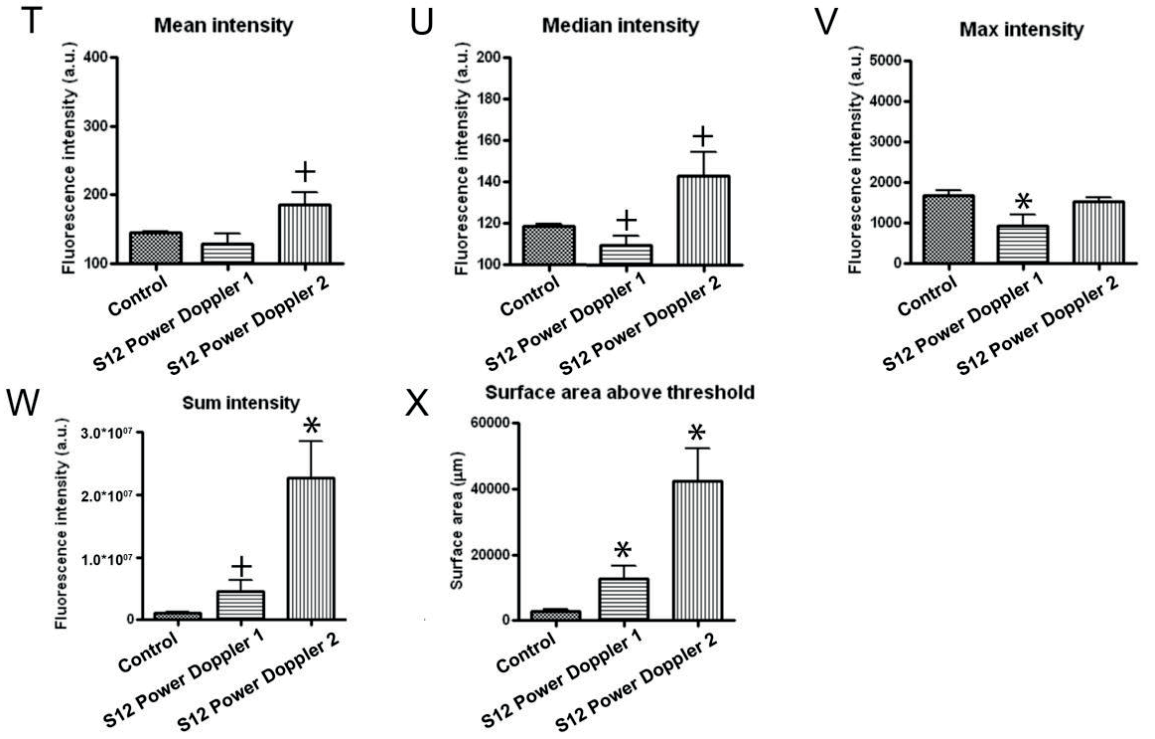

Figure 5 UTMD-triggered antagomir delivery to the healthy heart after 48 h. *A–C) Montage images of hearts extracted 30min after treatment, stained with wheat germ agglutinin (green) and DAPI (blue), antagomir is visualized in red. Arrows point toward the part of the heart where the UTMD effect was observed. Size bar=1mm. D) Images of cellular antagomir delivery after S12 Power Doppler 1 (D+E) and S12 Power Doppler 2 (F+G) protocols. Solid line arrows point toward intracellular delivery of antagomir with undisturbed cardiomyocyte morphology. Arrowheads point toward intracellular delivery of antagomir accompanied by an increased density of nuclei. Size bar=100 µm. H–K) High magnification images of cellular delivery pattern of UTMD using the S12 Power Doppler 2 protocol, stainedwith wheat germ agglutinin (green) and DAPI (blue), antagomir is visualized in red. Solid line arrows point toward intracellular delivery of antagomir with undisturbed cardiomyocyte morphology. Arrowheads point toward intracellular delivery of antagomir accompanied by an increased density of nuclei. Size bar= 50 µm. L–O) Neutrophil staining (green) of S12 Power Doppler 2 treated mice with nuclei staining (blue) and antagomir in red. Size bar= 50 µm. E) TUNEL-staining (green) of S12 Power Doppler 2 treated mice. Nuclei are visualized in blue and antagomir in red. Size bar=50 µm. T–X) Quantification of fluorescence images. *p < 0.05, +p < 0.01 compared to control values. Amount of animals per group: control =4, S3 Power Doppler=4, S12 Power Doppler 1 A=3, S12 Power Doppler 2 B=6. Control animals received an i.v. injection of antagomir only and were treated with the S3 Power Doppler protocol.*

Quantification of local delivery (48 h)

Quantification of microscopic images of hearts taken after 48 h showed that the increased delivery persisted for 48 h (Fig. 5T–X). The original S12 Power Doppler 1 protocol showed no effect on Mean intensity (Fig. 5T) and Median intensity (Fig. 5U) and a decrease in Max intensity (Fig. 5V), indicating an effect of UTMD on delivery patterns. The S12 Power Doppler 1 protocol also showed an increase in Sum intensity (Fig. 5W) and Surface area above threshold (Fig. 5X) compared to controls, indicating increased delivery of antagomir. Control

values for total amount of antagomir presence were comparable to the levels of 24 h; however, this was distributed over a smaller area, resulting in higher values for Mean intensity, Median intensity and Max intensity. This is probably the reasons why at 24 h the S12 Power Doppler 1 protocol does not cause significant increases in these parameters compared to controls. The S12 Power Doppler 2 protocol, with increased US intensity, displayed the most consistent delivery results and showed the highest Sum intensity (Fig. 5W) and Surface area above the threshold (Fig. 5X), which indicates increased delivery of absolute amounts of antagomir. Furthermore, the S12 Power Doppler 2 protocol showed a trend to increase Mean intensity (Fig. 5T) and Median intensity (Fig. 5U). This means that both S12 Power Doppler protocols had an effect on delivery pattern of antagomir as well as an effect on absolute delivery of antagomir, which was increased.

The immediate effect of treatment on cardiac function

ECG

UTMD had an effect on the ECG during and shortly after treatment. However, only in the treatment group S12 Power Doppler 2, where hearts were extracted at the 48 h time point, all mice showed an effect of UTMD on the ECG. In all other groups, only a subset of treated mice showed ECG-alterations, therefore only the effect on ECG in the S12 Power Doppler 2 group are displayed. UTMD affected the QRS-voltages, indicative for a ventricular conduction delay, probably due to changes in volume and form of the left ventricle. Additionally, ECG-alterations during treatment were a predictor of antagomir delivery. In all animals where antagomir delivery to the heart was increased, ECG-alterations were observed. Similarly, if ECG alternations were not observed, antagomir delivery to the heart was also absent.

Cardiac and respiratory functions

UTMD had an immediate effect on cardiac function as measured in M-mode echocardiography (Fig. 6). UTMD decreased diastolic diameter and calculated diastolic volume of the left ventricle for both the S12 and S3 Power Doppler treatment protocols ($p < 0.05$). Furthermore, there was a trend toward a decrease in systolic diameter and volume using the S3 Power Doppler protocol. Additionally, UTMD showed a trend toward an increase in ejection fraction and fractional shortening for the S3 Power Doppler protocol ($p < 0.1$). Finally, UTMD increased anterior wall thickness, both in systole and diastole ($p < 0.05$) and posterior wall thickness in systole ($p < 0.05$). During treatment, some mice showed respiration difficulties when treated with the S3 or S12 Power Doppler protocols. After sacrificing and autopsy of these mice, pulmonary hemorrhaging was observed. In none of the mice petechiae on the hearts were observed.

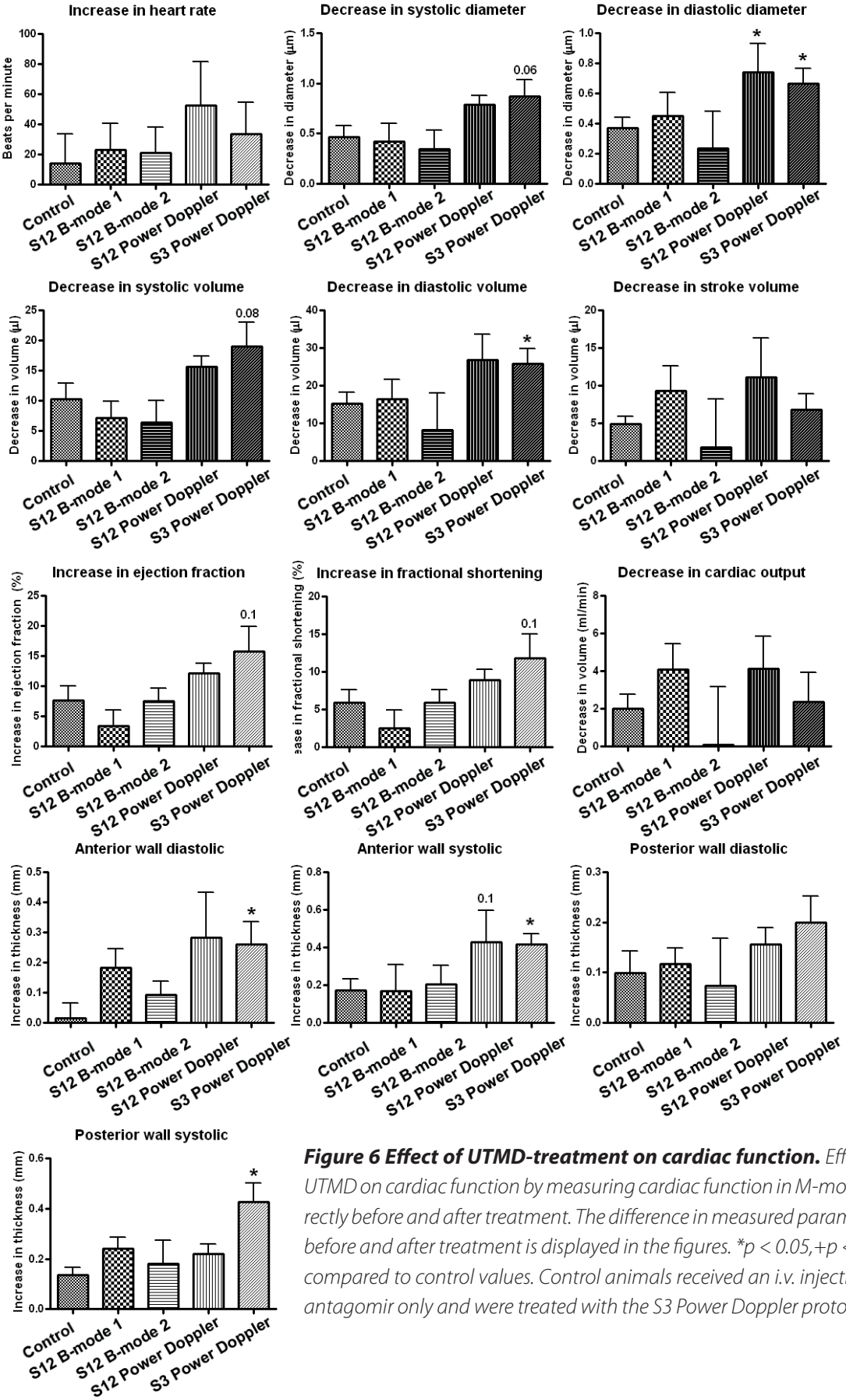

Figure 6 Effect of UTMD-treatment on cardiac function. *Effect of UTMD on cardiac function by measuring cardiac function in M-mode directly before and after treatment. The difference in measured parameters before and after treatment is displayed in the figures. *p < 0.05,+p < 0.01 compared to control values. Control animals received an i.v. injection of antagomir only and were treated with the S3 Power Doppler protocol.*

Myocardial contraction patterns (movie clips)

In addition to changing cardiac function as measured by M-mode, UTMD with the S3 and S12 Power Doppler treatment protocols also directly affected the contraction pattern of the heart. After treatment, the left anterior wall of the heart showed a delay in contraction compared to the rest of the heart. This was however completely normalized 24 h after treatment, suggesting a temporal acute effect.

Troponin I levels

UTMD treatment did not statistically significantly increase Troponin I levels of specific treatment groups at 30 min (Fig. 7A). Quantification of antagomir delivery was correlated with troponin I levels and we found a statistically significant correlation of Mean intensity, Median intensity and Sum intensity with troponin I levels ($p < 0.05$, Fig. 7B). This indicates that profound delivery of antagomir was associated with increased levels of troponin I in the blood. After 24 h and 48 h, Troponin I levels were at control levels in all treatment groups and mice (Fig. 7A).

Delivery of antagomiR to the I/R myocardium

As the S12 Doppler 2 protocol gave the best results for antagomir delivery in the healthy heart, this protocol was used for the treatment of I/R mouse hearts.

30 min after treatment

Surprisingly, 30 min after I/R, antagomir delivery to the myocardium without UTMD was profound and similar in both control (Fig. 8A+B) and UTMD treated hearts (Fig 8C+D). This is in strong contrast to healthy control hearts from the earlier experiments (Fig. 6A). Cellular distribution patterns of antagomir in both I/R control and I/R UTMD hearts was comparable to antagomir distribution as a result of UTMD in the healthy heart (Fig. 8E–H).

Localization of antagomiR (24 h)

After 24 h, the antagomir could still be found in the heart both in control (Fig. 8I+J) and UTMD-treated animals (Fig. 8K+L) in the infarcted areas. Antagomir was located inside the cardiomyocytes (Fig. 8M–P), with comparable morphology as the UTMD-triggered delivered antagomir in the healthy myocardium. Clear intracellular presence of antagomir could be observed inside cardiomyocytes. Additionally, intracellular antagomir delivery was associated with the influx of cells (Fig. 8N). Not surprisingly, these cells were identified as neutrophils (Fig. 6Q–T, arrows), as to be expected 24 h after I/R. No difference between control hearts and UTMD treated hearts was observed. Additionally, TUNEL staining confirmed

the presence of apoptosis (Fig. 8U–X, arrows). Both apoptosis and neutrophil infiltration could mainly be found in areas that contained antagomir inside cardiomyocytes, this area is very likely the area of I/R, even though with the applied staining this cannot be concluded definitively.

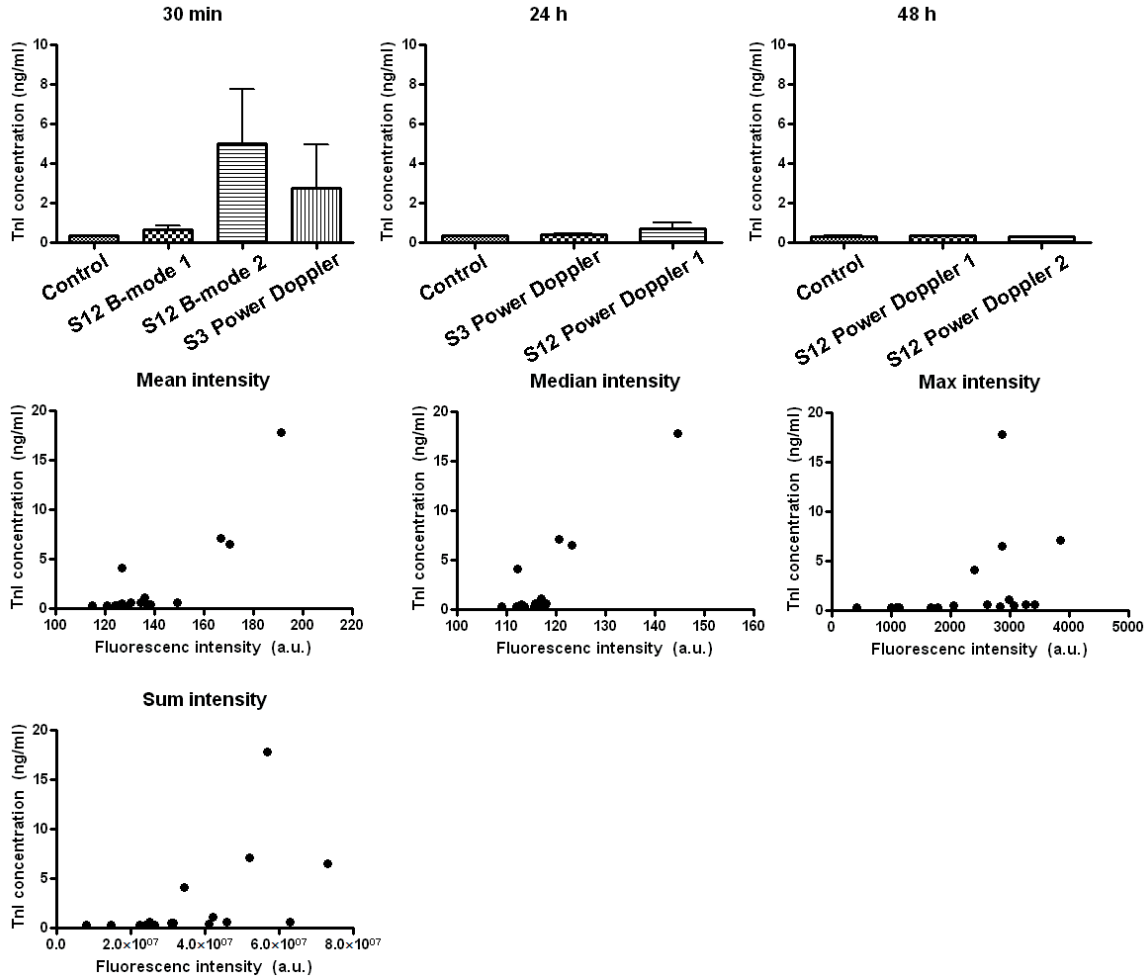

Figure 7 Effect of UTMD-treatment on Troponin I release. *A) Troponin I levels in the blood after 30min, 24 h and 48 h. B) Correlation of troponin I levels in the blood at 30min with quantification markers for antagomir delivery.*

Quantification of local delivery

Compared to healthy untreated hearts, I/R itself resulted in a significant increase in Mean intensity (Fig. 8Y), Median intensity (Fig. 8Z), Max intensity (Fig. 8AA), Sum intensity (Fig. 8AB) and Surface area (Fig. 8AC) at 24 h ($p < 0.05$). No further effect of UTMD on antagomir delivery was observed. At 30 min, a non-significant increase was observed.

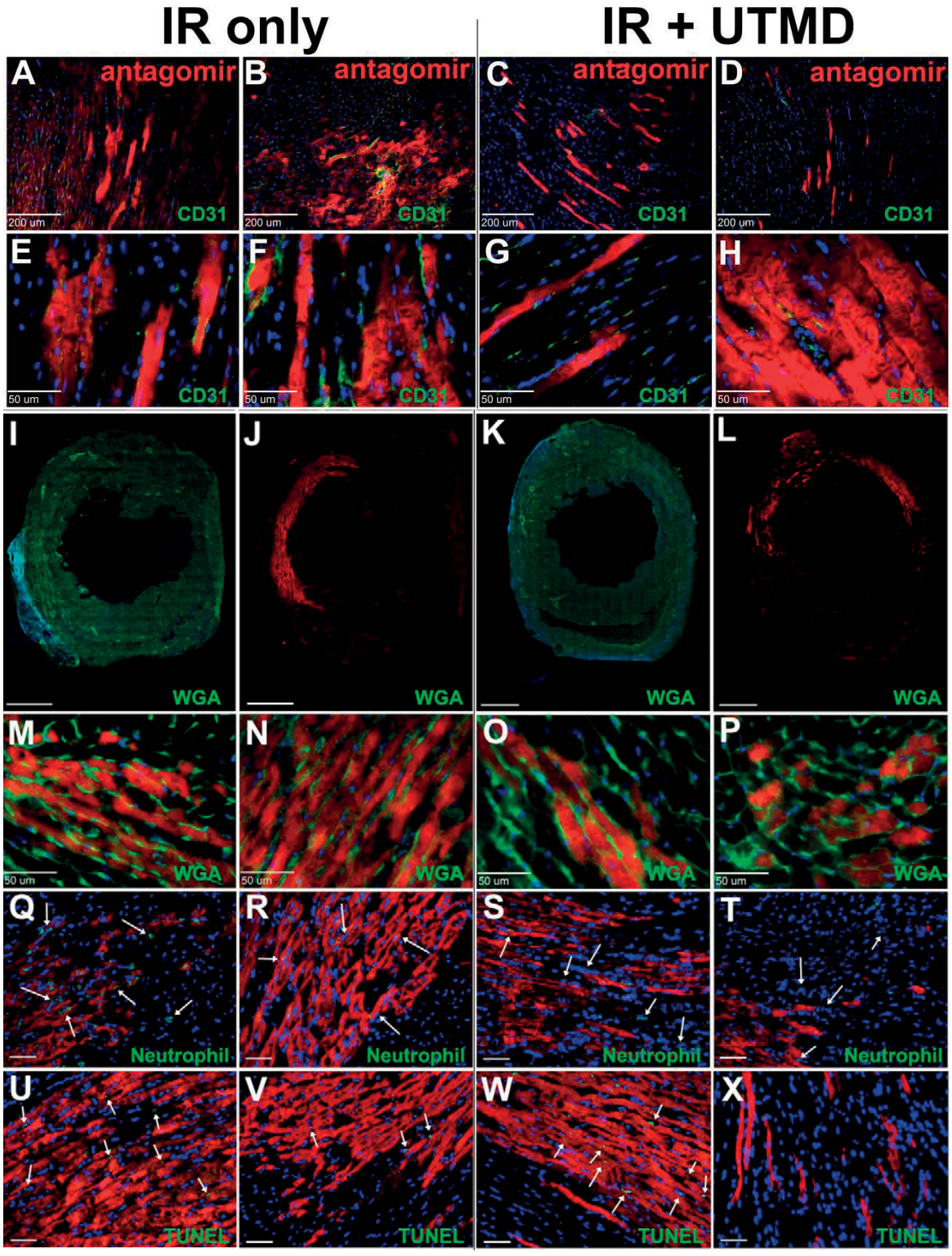
IR only
IR + UTMD
A antagomir
CD31
200 um
B antagomir
CD31
200 um
C antagomir
CD31
200 um
D antagomir
CD31
200 um
E
CD31
50 um
F
CD31
50 um
G
CD31
50 um
H
CD31
50 um
I
WGA
J
WGA
K
WGA
L
WGA
M
WGA
50 um
N
WGA
50 um
O
WGA
50 um
P
WGA
50 um
Q
Neutrophil
R
Neutrophil
S
Neutrophil
T
Neutrophil
U
TUNEL
V
TUNEL
W
TUNEL
X
TUNEL

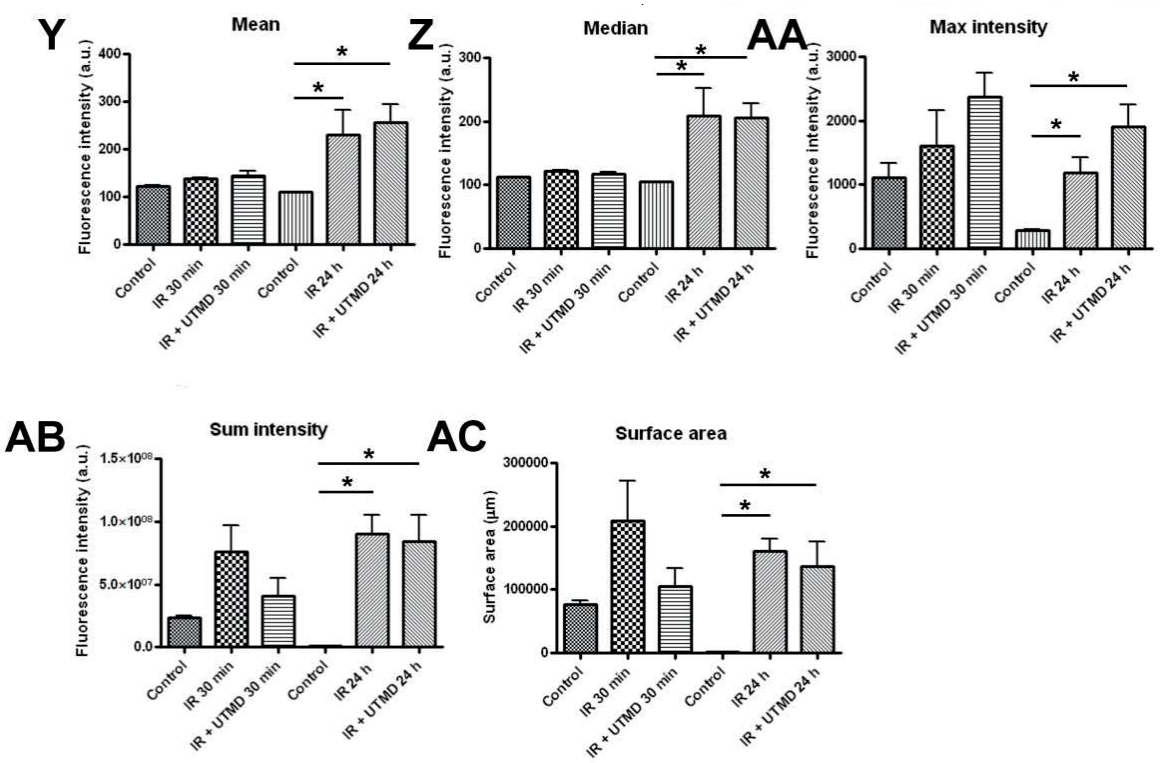

Figure 8 UTMD-triggered antagomir delivery in the heart after ischemia reperfusion. *A–D) 100× magnification images of control (A+B) and UTMD-treated heart after (C+D) extracted 30 min after IR, stained with wheat germ agglutinin (green) and DAPI (blue), antagomir is visualized in red. Size bar = 200 µm. E–H) 400× magnification images of control hearts (E+F) and IR heart (G+H) extracted 30 min after reperfusion, stained with wheat germ agglutinin (green) and DAPI (blue), antagomir is visualized in red. Size bar=50 µm. I–J)Montage images of hearts extracted 24 h after IR, either after control treatment (I+J) or UTMD (K+L), stained with wheat germ agglutinin (green) and DAPI (blue), antagomir is visualized in red. Size bar=1mm. M–P) High-magnification images of infarcted area with antagomir-uptake in cardiomyocytes 24 h after IR in control-treated (M+N) and UTMD (O+P) hearts, stained with wheat germ agglutinin (green) and DAPI (blue), antagomir is visualized in red. Size bar=50 µm. Q–T) Neutrophil staining (green) 24 h after IR in control-treated (Q+R) or UTMD (S+T) hearts (nuclei in blue, antagomir in red). Size bar=50 µm. U–X) TUNEL staining (green) for apoptosis in IR hearts 24 h after control-treatment (U+V) or UTMD (W+X) (nuclei in blue, antagomir in red). Size bar=50 µm. Y–AC) Quantification of antagomir presence in IR-hearts. *p < 0.05. Amount of animals per group: Control 30 min=6, IR 30 min=4, IR+UTMD 30 min=4, Control 24 h=5, IR 24 h=4, IR+UTMD 24 h=4. Control animals underwent ischemia–reperfusion (IR), received an i.v. injection of antagomir only andwere treated with the S3 Power Doppler protocol.*

Discussion

The present study shows that UTMD increases cardiac delivery of antagomir and changes the delivery pattern, when using US-protocols employing different imaging modes and frequencies. One of the major new findings is that UTMD can increase local antagomir delivery to the heart, and that a short stranded RNA (~22 base pairs) can be acutely delivered to the cardiomyocytes intracellularly. S12 Power Doppler 2, with a higher setting for depth and

focus compared to S12 Power Doppler 1, gave the most robust delivery results, probably due to the larger pulse length of emitted US and thus a higher intensity. Delivery occurs mostly to the anterior wall of the heart and the extent of delivery is dependent on US frequency and US mode. A higher frequency leads to a more restricted delivery to the anterior wall; a lower frequency reaches more parts of the heart. B-mode imaging protocols cause heterogeneous delivery patterns, in some mice delivering antagomir to capillaries and in other mice delivering antagomir into cardiomyocytes, Power Doppler protocols consistently deliver antagomirs into cardiomyocytes. This is probably caused by the higher amount of consecutive waves Power Doppler employs (6–8 pulses) compared to B-mode (2 pulses) within one US-pulse. B-mode imaging has the potential to cause similar effects but seems to operate at more of a threshold of US-energy that is needed, causing heterogeneous results. In addition to the groups reported in the Results section, more US-protocols were tested. Since these gave heterogeneous non-optimal results, we did not further explore these. However, we find it important to share those data and settings and these are included in the Supplementary data Fig. C. After treatment with Power Doppler protocols, antagomirs remain in the cardiomyocytes for up to at least 48 h. Some of the antagomir is internalized by cells that enter the heart after UTMD. A part of the cellular influx was identified as neutrophil granulocytes with molecular markers, non-identified cells might be monocytes or lymphocytes based on their morphology. Numbers of neutrophils remain the samefrom24 to 48 h and no apoptosis is present in the heart up to 48 h after UTMD. We thus conclude that any potential damaging effects of UTMDin the heart is local and temporal, and do not persist nor cause damage to the cardiomyocytes. The acute effects of UTMD on the heart include temporary alterations of the ECG and thickening of the left ventricular wall, also influencing left ventricular volumes and ejection fraction. A possible explanation is the occurrence of temporary myocardial edema or hypercontractility due to increased cardiac permeability, thereby influencing calcium levels inside cardiomyocytes [18]. Strikingly, after I/R, antagomirs enter cardiomyocytes in the infarcted region of the heart and we found that the cellular delivery pattern is similar to UTMD-deliver patterns. This finding points to the existence of a potential therapeutically accessible window of increase vascular permeability directly after I/R, in which antagomir delivery can be confined to the part of the heart that is affected by I/R. Clearly, further studies to fully explore this opportunity will be necessary.

Antagomirs have been successfully used in the past for cardiac applications. However, repetitive systemic doses used in those studies are high and range from 2.5–80 mg/kg body weight [19,20], making antagomir-treatment expensive. Additionally, antagomirs show low cardiac specificity [7]. Lowering the i.v. dose of antagomir has been tried but resulted in specific miR knockdown in endothelial cells [21]. Using UTMD, one can lower the dose but still deliver antagomir to cardiomyocytes, increasing possibilities for cell-specific treatment. One drawback is that UTMD-effects when using the S12 Power Doppler protocols are confined to the anterior wall of the heart. This is probably caused by US-energy absorbing

MBs in the left ventricle, as a results decreasing US-penetration and shielding the posterior wall. This is expected given the size distribution of the MB (~1–2 µm) as these are known to primarily absorb US waves at around 6–7 MHz. US-penetrance can be increased with an S3 transducer operating at a lower frequency (1.5 MHz), which causes less US-absorbance by MB and higher USpenetration. However, a lower frequency comes with a lower spatial resolution, making it difficult to position the transducer correctly over the mouse heart. Thiswill be less relevant in larger animals and humans where a lower spatial resolution is not an issue to correctly position the transducer over the heart. Additionally, a trans-esophageal transducer might be useful to treat specific parts of the heart by approaching the heart from different angles.

Even though UTMD has been used in the cardiac setting before, only little information is known about localization of delivered therapeutics in the heart [14,22]. Much work has been done in optimizing US parameters and MBs, and results have improved [11,12,23,24]. However, with a focus and technical details, the mechanism of delivery remains to be conclusively elucidated. In vitro data suggests that sonoporation, a temporal increased membrane permeability due to vibration of single MB, is the driving force behind increased delivery using UTMD [25]. If that were the mechanism involved, we would expect most delivery to the capillaries, increased vascular permeability and extravasation of antagomir to the interstitium. In this study, however, delivery is mainly achieved to cardiomyocytes. Additionally, we observed an on/off pattern of antagomir delivery to cardiomyocytes. If UTMD operates through a mechanism reliant on vibrations of single MB, with the amounts of MB present in the heart, we would expect a more continues delivery pattern. Sonoporation, an increased membrane permeability due to oscillations of single MB, does not seem to be the driving factor behind UTMD effects in the heart. We have not elucidated the precise mechanism of delivery, but rather revealed a unique and consistent delivery pattern in the heart, which is very different from delivery patterns in skeletal muscle and does not fit with sonoporation but points toward a mechanism that both increases vascular permeability and cardiomyocyte permeability, without influencing endothelial cell permeability [15,26].

One (other) concern with UTMD is potential damaging effects of MB destruction [27–30]. These effects include endothelial damage, vascular rupture and cardiomyocyte damage. Early work on MB-destruction showed that damaging effect can be managed by adjusting the US treatment protocol [28]. Since several US treatment protocols were tested in the present study, we also studied adverse effects of treatment on the heart.

We did indeed find comparable effects as previously described. Miller et al. in 2005 showed Evans blue localization inside cardiomyocytes after MB destruction [28], subsequently concluding that MB destruction causes cardiomyocyte damage. In the present study, antagomir delivery patterns to cardiomyocytes looked very similar to the intracellular Evans blue patterns. However, we found no apoptosis of cardiomyocytes and therefore conclude that this intracellular delivery pattern does not represent damage but localized delivery of

a therapeutic agent. We did not specifically test for endothelial damage or vascular rupture. However, no apoptosis of endothelial cells nor extravasation of red blood cells was observed, neither petechiae on the heart. We conclude that no persisting adverse effects were caused by UTMD in healthy hearts. We did find acute effects of UTMD on cardiac function and ECG that disappeared within 24 h and 5 min, respectively. UTMD increased ventricle wall thickness, influenced contraction pattern and decreased both systolic and diastolic volumes, clearly affecting cardiac function. Although this was not fatal in the animals presented in this study, some animals in the Power Doppler groups did show respiratory difficulties during treatment. After treatment, this disappeared within 5 min. We speculate that the effect of UTMD on cardiac function causes a lower cardiac output, which could cause fluid buildup and edema in the lung. As fluids allow US propagation through the lung and air does not, in the case of pulmonary edema, US is propagated through the lungs and can cause MBs to explode in the pulmonary vasculature causing micro vessels to rupture. This can result in pulmonary hemorrhaging in those mice. We believe that this effect is specific for this animal model, as the US-transducers are designed for human use where the lungs are positioned farther away from the heart so that US-energy does not penetrate to this depth.

Another major finding of our study is that I/R itself allows antagomirs to enter cardiomyocytes within 30 min after reperfusion. This provides a potential strategy to specifically deliver antagomir to the infarcted area by injecting antagomir within 5 min of reperfusion. UTMD does not have an additional effect on antagomir delivery. Both UTMD and I/R are known to increase vascular permeability in the heart, causing antagomir to leave the blood vessel. Why antagomir subsequently can enter cardiomyocytes this easily within 30 min is unclear. In in vitro studies we experienced that antagomirs do enter cells on their own, but this typically takes hours, not 30 min. Our results indicate that in parallel with increased vascular permeability, cellular permeability of cardiomyocytes also increases. The mechanism underlying this combined increased microvascular and cardiomyocyte permeability is still unknown, but clearly deserves renewed investigation. Since UTMD and I/R show similar antagomir uptake patterns, we hypothesize that the mechanism that drives uptake after UTMD might be caused by I/R stress to the cardiomyocytes, leading to temporary and reversible membrane permeabilization.

In conclusion, the present study shows that UTMDcan locally deliver antagomir into the cardiomyocytes of the heart without causing persistent damage. The antagomir remains in the cardiomyocytes for over 48 h. The best results are obtained with an S12 transducer operating in Power Doppler mode, causing local antagomir delivery to the anterior wall of the heart as the MB-filled ventricle shields the posterior part. This study is the first to explore cardiac antagomir delivery using UTMD. In addition, it is the first to study tissue distribution of short RNA based therapeutics (~22 base pairs) at both the cellular and organ levels after UTMD to the heart in general. Interestingly, I/R itself provides a disease-associated targeting mechanism to locally deliver antagomir to the infarcted heart much like the increased reten-

tion and enhanced permeability mechanism in tumors. As the delivery pattern caused by I/R is similar to UTMD-triggered delivery of antagomir, the underlying mechanism might also be related to — and probably involves — short-term, non-damaging (reversible), ischemia or reperfusion triggered events. These findings may be beneficial for developing therapeutical inhibition of myocardial apoptosis and promoting cardiomyocyte survival after cardiac I/R. Overall, UTMD is most suited to manipulate miRNA-function and subsequent processes like apoptosis, proliferation and/or hypertrophy in cardiomyocytes in the later stages after myocardial infarction or in more chronic cardiac diseases like hypertrophic cardiomyopathy or chronic heart failure.

Acknowledgements

We thank Zhiyong Lei, Janine Deddens and Dries Feyen for their suggestions and technical assistance on the experiments represented in this study. We also acknowledge Sharyn Roodenburg for her assistance in MB creation and validation. This research forms part of the Project P1.05 LUST of the research program of the BioMedical Materials institute, co-funded by the Dutch Ministry of Economic Affairs. We furthermore gratefully acknowledge the financial support of the Netherlands CardioVascular Research Initiative (CVON): The Dutch Heart Foundation, Dutch Federation of UniversityMedical Centers, The Netherlands Organization for Health Research and Development, and the Royal Netherlands Academy of Sciences.

REFERENCES

[1] A.E. Pasquinelli, B.J. Reinhart, F. Slack, M.Q. Martindale, M.I. Kuroda, B. Maller, D.C. Hayward, E.E. Ball, B. Degnan, P. Muller, J. Spring, A. Srinivasan, M. Fishman, J. Finnerty, J. Corbo, M. Levine, P. Leahy, E. Davidson, G. Ruvkun, Conservation of the sequence and temporal expression of let-7 heterochronic regulatory RNA, Nature 408 (2000) 86–89.

[2] E.M. Small, R.J. Frost, E.N. Olson, MicroRNAs add a new dimension to cardiovascular disease, Circulation 121 (2010) 1022–1032.

[3] Z. Lei, J.P. Sluijter, A. Mil, MicroRNA therapeutics for cardiac regeneration, Mini Rev. Med. Chem. 15 (2015) 441–451.

[4] J. Krutzfeldt, N. Rajewsky, R. Braich, K.G. Rajeev, T. Tuschl, M. Manoharan,M. Stoffel, Silencing of microRNAs in vivo with 'antagomirs', Nature 438 (2005) 685–689.

[5] X.P. Ren, J.Wu, X.Wang, M.A. Sartor, J. Qian, K. Jones, P. Nicolaou, T.J. Pritchard, G.C. Fan, MicroRNA-320 is involved in the regulation of cardiac ischemia/reperfusion injury by targeting heat-shock protein 20, Circulation 119 (2009) 2357–2366.

[6] T. Thum, C. Gross, J. Fiedler, T. Fischer, S. Kissler, M. Bussen, P. Galuppo, S. Just, W. Rottbauer, S. Frantz, M. Castoldi, J. Soutschek, V. Koteliansky, A. Rosenwald, M.A. Basson, J.D. Licht, J.T. Pena, S.H. Rouhanifard, M.U. Muckenthaler, T. Tuschl, G.R. Martin, J. Bauersachs, S. Engelhardt, MicroRNA-21 contributes tomyocardial disease by stimulating MAP kinase signalling in fibroblasts, Nature 456 (2008) 980–984.

[7] H. Wang, M. Chiu, Z. Xie, M. Chiu, Z. Liu, P. Chen, S. Liu, J.C. Byrd, N. Muthusamy, R. Garzon, C.M. Croce, G. Marcucci, K.K. Chan, Synthetic microRNA cassette dosing: pharmacokinetics, tissue distribution and bioactivity, Mol. Pharm. 9 (2012) 1638–1644.

[8] R.V. Shohet, S. Chen, Y.T. Zhou, Z. Wang, R.S. Meidell, R.H. Unger, P.A. Grayburn, Echocardiographic destruction of albumin microbubbles directs gene delivery to the myocardium, Circulation 101 (2000) 2554–2556.

[9] P. Li, W.F. Armstrong, D.L. Miller, Impact of myocardial contrast echocardiography on vascular permeability: comparison of three different contrast agents, Ultrasound Med. Biol. 30 (2004) 83–91.

[10] B.D. Meijering, L.J. Juffermans, A. van Wamel, R.H. Henning, I.S. Zuhorn, M. Emmer, A.M. Versteilen, W.J. Paulus, W.H. van Gilst, K. Kooiman, N. de Jong, R.J. Musters, L.E. Deelman, O. Kamp, Ultrasound and microbubble-targeted delivery of macromolecules is regulated by induction of endocytosis and pore formation, Circ. Res. 104 (2009) 679–687.

[11] S. Chen, J. Chen, P. Huang, X.L. Meng, S. Clayton, J.S. Shen, P.A. Grayburn, Myocardial regeneration in adriamycin cardiomyopathy by nuclear expression of GLP1 using ultrasound targeted microbubble destruction, Biochem. Biophys. Res. Commun. (2015).

[12] P. Yan, K.J. Chen, J.Wu, L. Sun, H.W. Sung, R.D.Weisel, J. Xie, R.K. Li, The use ofMMP2 antibody-conjugated cationic microbubble to target the ischemic myocardium, enhance Timp3 gene transfection and improve cardiac function, Biomaterials 35 (2014) 1063–1073.

[13] Q.Y. Yuan, J. Huang, B.C. Chu, X.J. Li, X.S. Li, L.Y. Si, A targeted high-efficiency angiogenesis strategy as therapy for myocardial infarction, Life Sci. 90 (2012) 695–702.

[14] S. Tsunoda, O. Mazda, Y. Oda, Y. Iida, S. Akabame, T. Kishida, M. Shin-Ya, H. Asada, S. Gojo, J. Imanishi, H. Matsubara, T. Yoshikawa, Sonoporation usingmicrobubble BR14 promotes pDNA/siRNA transduction to murine heart, Biochem. Biophys. Res. Commun. 336 (2005) 118–127.

[15] R.F. Kwekkeboom, Z. Lei, S.J. Bogaards, E. Aiazian, O. Kamp, W.J. Paulus, J.P. Sluijter, R.J. Musters, Ultrasound and microbubble-induced local delivery of MicroRNAbased therapeutics, Ultrasound Med. Biol. 41 (2015) 163–176.

[16] A. van Mil, S. Grundmann, M.J. Goumans, Z. Lei, M.I. Oerlemans, S. Jaksani, P.A. Doevendans, J.P. Sluijter, MicroRNA-214 inhibits angiogenesis by targeting quaking and reducing angiogenic growth factor release, Cardiovasc. Res. 93 (2012) 655–665.

[17] M.I. Oerlemans, J. Liu, F. Arslan, K. den Ouden, B.J. van Middelaar, P.A. Doevendans, J.P. Sluijter, Inhibition of RIP1-dependent necrosis prevents adverse cardiac remodeling after myocardial ischemia–reperfusion in vivo, Basic Res. Cardiol. 107 (2012) 270.

[18] W.E. Louch, M.K. Stokke, I. Sjaastad, G. Christensen, O.M. Sejersted, No rest for the weary: diastolic calcium homeostasis in the normal and failing myocardium, Physiology 27 (2012) 308–323.

[19] A. Sengul, R. Santisuk,W. Xing, C. Kesavan, Systemic administration of an antagomir designed to inhibit miR-92, a regulator of angiogenesis, failed to modulate skeletal anabolic response to mechanical loading, Physiol. Res. 62 (2013) 221–226.

[20] T. Thum, MicroRNA therapeutics in cardiovascular medicine, EMBO Mol. Med. 4 (2011) 3–14.

[21] J. Fiedler, V. Jazbutyte, B.C. Kirchmaier, S.K. Gupta, J. Lorenzen, D. Hartmann, P. Galuppo, S. Kneitz, J.T. Pena, C. Sohn-Lee, X. Loyer, J. Soutschek, T. Brand, T. Tuschl, J. Heineke, U. Martin, S. Schulte-Merker, G. Ertl, S. Engelhardt, J. Bauersachs, T. Thum, MicroRNA-24 regulates vascularity after myocardial infarction, Circulation 124 (2011) 720–730.

[22] H. Fujii, S.H. Li, J. Wu, Y. Miyagi, T.M. Yau, H. Rakowski, K. Egashira, J. Guo, R.D. Weisel, R.K. Li, Repeated and targeted transfer of angiogenic plasmids into the infarcted rat heart via ultrasound targeted microbubble destruction enhances cardiac repair, Eur. Heart J. 32 (2011) 2075–2084.

[23] S. Chen, M. Shimoda, J. Chen, P.A. Grayburn, Stimulation of adult resident cardiac progenitor cells by durable myocardial expression of thymosin beta 4 with ultrasound-targeted microbubble delivery, Gene Ther. 20 (2013) 225–233.

[24] S. Chen, R.V. Shohet, R. Bekeredjian, P. Frenkel, P.A. Grayburn, Optimization of ultrasound parameters for cardiac gene delivery of adenoviral or plasmid deoxyribonucleic acid by ultrasound-targeted microbubble destruction, J. Am. Coll. Cardiol. 42 (2003) 301–308.

[25] B. Geers, H. Dewitte, S.C. De Smedt, I. Lentacker, Crucial factors and emerging concepts in ultrasound-triggered drug delivery, J. Control. Release 164 (2012) 248–255.

[26] H. Leong-Poi, M.A. Kuliszewski, M. Lekas, M. Sibbald, K. Teichert-Kuliszewska, A.L. Klibanov, D.J. Stewart, J.R. Lindner, Therapeutic arteriogenesis by ultrasoundmediated VEGF165 plasmid gene delivery to chronically ischemic skeletal muscle, Circ. Res. 101 (2007) 295–303.

[27] D.L. Miller, E.M. Driscoll, C. Dou, W.F. Armstrong, B.R. Lucchesi, Microvascular permeabilization and cardiomyocyte injury provoked by myocardial contrast echocardiography in a canine model, J. Am. Coll. Cardiol. 47 (2006) 1464–1468.

[28] D.L. Miller, P. Li, C. Dou, D. Gordon, C.A. Edwards, W.F. Armstrong, Influence of contrast agent dose and ultrasound exposure on cardiomyocyte injury induced by myocardial contrast echocardiography in rats, Radiology 237 (2005) 137–143.

[29] R.J. Price, D.M. Skyba, S. Kaul, T.C. Skalak, Delivery of colloidal particles and red blood cells to tissue through microvessel ruptures created by targeted microbubble destruction with ultrasound, Circulation 98 (1998) 1264–1267.

[30] D.M. Skyba, R.J. Price, A.Z. Linka, T.C. Skalak, S. Kaul, Direct in vivo visualization of intravascular destruction of microbubbles by ultrasound and its local effects on tissue, Circulation 98 (1998) 290–293.